David Karl, Ben Jastram, Paul H. Kamm, Hartmut Schwandt, Aleksander Gurlo, Franziska Schmidt

Porous polylactide-co-glycolide / bioactive glass composite microsphere powders for laser sintering of scaffolds

Citation details
Karl, D., Jastram, B., Kamm, P. H., Schwandt, H., Gurlo, A., & Schmidt, F. (2019). Evaluating porous polylactide-co-glycolide/bioactive glass composite microsphere powders for laser sintering of scaffolds. In Powder Technology (Vol. 354, pp. 289–300). Elsevier BV. https://doi.org/10.1016/j.powtec.2019.06.010.

Porous polylactide-co-glycolide / bioactive glass composite microsphere powders for laser sintering of scaffolds

David Karl,[1]* Ben Jastram,[2] Paul H. Kamm,[3] Hartmut Schwandt,[2] Aleksander Gurlo[1] and Franziska Schmidt[1]

Affiliations:

[1] Fachgebiet Keramische Werkstoffe / Chair of Advanced Ceramic Materials, Institut für Werkstoffwissenschaften und –technologien, Technische Universitaet Berlin, Hardenbergstrasse 40, 10623 Berlin, Germany

[2] 3D Labor, Institut fuer Mathematik, Technische Universitaet Berlin, Strasse des 17. Juni 135, 10623 Berlin, Germany

[3] Institute of Applied Materials, Helmholtz-Zentrum Berlin für Materialien und Energie, Hahn-Meitner-Platz 1, 14109 Berlin, Germany

*Correspondence to: david.karl@ceramics.tu-berlin.de

Abstract

While laser sintering (LS) processes are typically optimised towards denser powder beds, our approach is different as we investigate the use of non-dense powder beds made of porous composite powder materials of polylactide-co-glycolide (PLGA) and bioactive glass (BG) 45S5. Powders were produced via solid-in-oil-in-water emulsion with different BG modifications as porogen, changing PLGA:BG ratios and subsequently used in LS. The powders and LS parts were characterised using SEM(/EDX), FTIR, XRD, XRF, TG, powder packing and flow properties, PSD and X-ray tomography. The microparticles showed varying degrees of sphericity, porosity and SSA while the BG porogen could be incorporated into or onto the foamed polymer. Powders were used for LS and gave LS parts with extra porous structures. While the powders could be useful for various applications in medicine our special LS approach might be interesting were multiple feedstock powders are used and or to generate extra porous tissue engineering scaffolds.

Abbreviations: AM - Additive Manufacturing; BG - bioactive glass; DCM - dichloromethane; DDW - double-deionised water; DW - deionised water; HA - hydroxylapatite; LS - laser sintering; PGA - polyglycolide; PLA - polylactide; PLGA - polylactide-co-glycolide; PSD - particle-size distribution; PTES - n-Propyltriethoxysilane; PVA - polyvinyl alcohol; s/o/w - solid-in-oil-in-water; SSA - specific surface area;

Keywords: porous microspheres**;** laser sintering; tissue engineering scaffolds; PLGA; bioactive glass;

1. Introduction

The material of natural bone can be classified as a composite material - it is composed of an organic collagen matrix with a particle reinforcement made of inorganic minerals. To produce synthetic bone crafts, researchers work on biomaterials made of different combinations of organic and inorganic composites to mimic the shape and composite structure of bone. Aiming for substitutes that should not cause inflammatory response in the body, not be carcinogenic, mechanically stable and best bioactive. Moreover, it is important that the implant should lead to bone regrowth - the material should ideally be osseointegrativ or better yet osteoconductive [1]. Another desirable feature of such materials is the ability to be combined with medication. In general, many of the polymer-based implants are biodegradable polymers which have been in clinical use for many years [2]. Often, they are the aliphatic polyesters polylactide (PLA) and polyglycolide (PGA) as well as their copolymers, polylactide-co-glycolide (PLGA). One important aspect of these materials is their thermoplastic nature, which makes it possible to process them with Additive Manufacturing (AM) technologies. A promising approach to improve unfavourable characteristics of pure aliphatic polyesters in respect to the adhesion of osteoblasts, their mechanical properties, and their acidic degradation are composites such as PLGA with inorganic particles like hydroxylapatite (HA) or bioactive glass (BG). Composite materials of such polymers with BG have drawn increasing attention as BG's ionic dissolution products have been shown to stimulate osteogenesis and angiogenesis [3]. In some areas BG has been proven to be favourable over HA – BG with the composition 45S5 (45 wt.%, SiO_2, 24.5 wt.% Na_2O, 24.5 wt.% CaO and 6 wt.% P_2O_5) has been found to stimulate the growth of bones to a greater extent than HA [4]. Also, BG is better suited as a carrier / delivery platform for therapeutic ions (eg Zn, Sr, Mg and Cu) [3]. Furthermore, by means of certain BG in composite materials, there is a buffering of the pH value on the polymer surface, which can be employed to tailor degradation behaviour [5]. Additive Manufacturing provides a number of advantages for the production of implants in comparison to conventional processes - with AM customizable geometries, based on individual medical image data, can be tailored to the individual patient and defect. One very

promising AM method is the laser sintering (LS) process that has the important advantage that components have very good mechanical properties and require little to no post-processing. Thanks to the self-stabilizing properties of the powder bed, no supporting structures are required, and there is no subsiding of structures. Another argument for the use of the LS to process biomaterials, besides it's good resolution, is the fact there being no need to use toxic substances as binder [6]. The standard approach using LS is to try to produce as dense as possible microstructures in the areas where the laser beam interacts with the particles, for which the packing density of the powder bed is an important parameter. The packing density is largely determined by morphology and particle size distribution of the used powder. Generally the best suited powder particles for ideal (dense), stable and reproducible packing are spherical in shape [7]. Furthermore, LS powders should not have a large fraction of very small particles as this would decrease their flowability.

In this work our approach is to produce non-dense powder beds using spherical composite particles for LS that have a foamed morphology on the inside e.g. a high particle porosity, to investigate the LS production of geometries / scaffolds with an extra high porosity. We aimed to first use the inorganic bioactive glass as a porogen to foam the resorbable polymer matrix with the bioactive glass incorporated into or onto the particles (to not decrease flowability for LS) and later fuse the bioactive glass into a dense polymer matrix using LS to produce composites with the aforementioned desirable biochemical properties.

2. Materials and methods

Composite microspheres were produced by a solid-in-oil-in-water (s/o/w) emulsion method (Figure 1) using dichloromethane (DCM) as solvent for the oil phase to dissolve PLGA and disperse the inorganic component bioactive glass 45S5 Bioglass® plus a water phase with polyvinyl alcohol (PVA) as emulsifier.

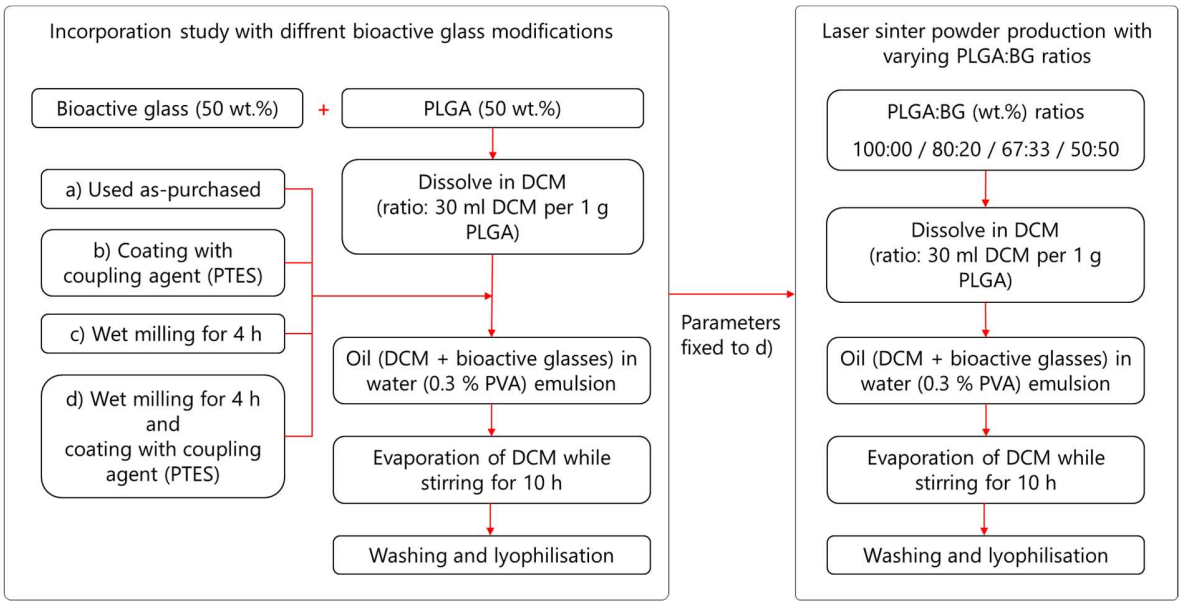

Figure 1: Flowchart of experimental procedure used to produce composite powders.

2.1 Production of composite microspheres

2.1.1 Bioactive glass modification

Melt-derived 45S5 Bioglass® was purchased (BG, Vyttrix, d_{50}=3.90 µm, Schott) and modified using wet milling and/or coating with a coupling agent, as described in the following two paragraphs.

2.1.2 Bioactive glass milling

BG was milled using the stirred media mill Attritor PE075 (Netzsch GmbH, Germany). 30 g of BG were dispersed in 240 ml deionised water (DW) and milled at 2000 RPM for 30 minutes using 490 g alumina balls with a diameter of 2.5 mm. The solution was centrifuged at 800 g for 10 min and the supernatant

was removed. The centrifugate was redispersed in 20 ml of DW, shock-frozen with liquid nitrogen and subsequently lyophilised.

2.1.3 Bioactive glass coating

n-Propyltriethoxysilane (PTES, >98 % deposition grade, Sigma-Aldrich) coupling agent was applied to the surface of non-milled and milled BG following a procedure described by Jiang et al. [8]. One percent (wt.%) PTES in aqueous solution was prepared using double-deionised water (DDW). Before preparation of the solution the pH value of DDW was adjusted to pH 3.5 using 100 % acetic acid. The different BG powders were added to the solution in a ratio of 1:18 respectively. Every sample was stirred for 2 hours at 200 RPM using a magnetic stirrer. In order to remove excess silane a similar volume of DDW was added (doubling the volume) and the solution was centrifuged at 800 g for 10 minutes after which the supernatant was removed. The centrifugate was redispersed in 20 ml of deionised water, shock-frozen with liquid nitrogen and subsequently lyophilised. The lyophilised powder was sieved using a 25-micron sieve. Finally, the powder was dried for a minimum of 48 hours at 80 °C in an oven without air circulation.

2.2 Solid in oil in water production of microspheres

2.2.1 Incorporation study

A solid-in-oil-in-water emulsion method at ambient temperature was established (Figure 1). As solid inorganic phase different BG modifications were prepared (BG as supplied (d_{50}=3.90 µm, BG milled (d_{50}=1.66 µm); BG coated (with PTES) and BG milled (d_{50}=1.66 µm) and coated (with PTES). For each of the four samples 4 g of PLGA (Resomer® RG755S, PLA:PGA ratio 75:25, Evonik) was dissolved in 120 ml dichloromethane (DCM, min. 99.8 % (stab.), Th.Geyer,) as the oil phase. In a next step 4 g of the respective BG was added to the solution and treated with the ultrasonic finger Sonifier 450 (Branson Ultrasonics Corp., USA) for 3 min to break up agglomerates. The mixtures were inserted into a specially designed titration device where the solutions were stirred from overhead during the titration process. The

oil phase was added dropwise at a speed of 3 ml/min into 1000 ml beakers filled with 400 ml of 0.3 % polyvinyl alcohol (PVA, >98 % hydrolysed, MW=72000, Merck) in water solution that was constantly being stirred at 490 RPM using magnetic stirring plates. After inserting the oil phase, emulsions were stirred at 490 RPM for 10 h to evaporate to solvent. Finally, the particles were collected by centrifugation (800 g), washed three times, frozen by placing the samples in a -80 °C freezer (Dairei Co.,Ltd., Japan) and subsequently lyophilised.

2.2.2 Composite powders with varying PLGA:BG ratios

To produce composite powders for LS-experiments the procedure above was repeated while changing the PLGA:BG ratios as well as double the sample amount.

Samples with PLGA:BG ratios of 50:50, 67:33, 80:20 and a sample with no BG (100:0) were produced. For each sample 8 g PLGA was dissolved in 240 ml DCM. For the samples 50:50, 67:33 and 80:20 the respective amounts of milled (d_{50}=1.61 µm) and PTES coated BG (8, 4 and 2 g) was mixed with the oily phase and treated with the ultrasonic finger. This oily phase was added dropwise to 800 ml of 0.3 % PVA solution that was stirred at 710 RPM. All other production parameters were kept similar to the above described production route. After washing and lyophilisation the resulting powders were sieved using a 100 µm sieve.

2.2.3 Laser sintering

The cuboid specimens (dimensions of 25 × 4 × 3 mm) were sintered using a modified Formiga P100 (EOS GmbH, Germany) laser sintering machine that is equipped with a CO_2 Laser with a diameter of the focused beam < 0.5 mm. A custom-made build chamber was used to produce test geometries for the composite particles in nitrogen atmosphere at ambient temperature with a layer thickness of 150 µm. Theses samples were built scanning with of 2,4 – 2,8 m/s at 16,8 W for hatching, upskin, downskin and 1,5 m/s at 12,8 W for contour, edges using a hatch distance of 0,25 mm. After fabrication the samples were carefully removed from the build chamber and cleaned using compressed air.

2.3 Characterization

Powder morphologies were investigated by scanning electron microscopy (SEM) using a XL20 (Philips N.V., Netherlands) at 10 kV acceleration voltage. The powders were fixed to a sample holder with adhesive carbon tape and subsequently sputter coated with gold. In addition, the incorporation of the inorganic phase was investigated by SEM coupled with energy dispersive X-ray spectroscopy (SEM/EDX) using a Gemini Leo 1530 (Carl Zeiss Microscopy GmbH, Germany) with acceleration voltage ranging from 5 to 10 kV, an in-lens and secondary electron (SE2) detector and a coupled EDX system (Thermo Fisher Scientific Inc., USA). The analysis of EDX data was performed with the NSS software version 4.1 from Thermo Fisher. Particle size distribution was investigated using a Helos H1505 laser diffraction device with wet dispersion unit Sucell2 (Sympatec GmbH, Germany). Changes in surface composition of the inorganic phase were studied by attenuated total reflection fourier transformed infrared spectroscopy (ATR/FT-IR) with an Equinox 55 (Bruker Corporation, USA) at 1 cm^{-1} resolution ranging from 4000 to 400 cm^{-1}. X-ray fluorescence was performed by a Panalytical PW2400 X-ray spectrometer (XRF) with autosampler, (Philips N.V., Netherlands). The specific surface area (SSA) of the powders was analysed by nitrogen adsorption using a Quadrasorb station (Quantachrome Instruments, USA) and determined by the Brunnauer, Emmet and Teller (BET) method. Powder packing and flow properties were evaluated by measuring the untapped bulk density ρ_{bulk} and the tapped bulk density ρ_{tapped} to calculate the Hausner ratio $HR = \frac{\rho_{tapped}}{\rho_{bulk}}$ [9]. For this all powders were dried using vacuum for at least 24 hours and the untapped bulk density was measured in a scaled down version of DIN EN ISO 60:1999 [10] using a 10 ml measuring cylinder. Subsequently the tapped density was measured by tapping the measuring cylinder 100-fold. All measurements were repeated threefold and averaged.

Thermogravimetric (TG) and differential thermal analysis (DTA) on powders were performed using STA409 PC / PG (Netzsch GmbH, Germany) with an Al_2O_3 crucible. Samples were heated in an air atmosphere from 25 to 600 °C at a heating rate of 10 K/min. X-ray tomographic white beam imaging was performed at the 7T-MPW-EDDI (Energy Dispersive DIffraction) beamline of the BESSY II synchrotron

radiation facility, Berlin, Germany [11]. Tomograms were acquired within 10 s over 180 ° using a 200 µm thick LuAG:Ce scintillator and a pco.dimax high speed CMOS camera (PCO AG, Germany) equipped with a macro lens with an optical magnification of ~4.4 resulting in a pixel size of 2.5 µm. The field of view was set to 4 mm × 2 mm by a beam slit system and reconstructions were performed using the ASTRA toolbox and a filtered back projection algorithm [12]. The obtained volumetric data was post-processed with the commercial software Avizo (FEI Company, USA) which included filtering and binarisation to segment the grey values into porosity and material. The closed porosity was separated from the open one by using morphological operations on the binarised data.

3. Results

3.1 Bioactive glass modification

As-purchased 45S5 powder showed a plate like particle morphology with a variation of particles sizes, as shown in Figure 2a. PTES coating led to similar particle morphology and rougher particle surfaces (Figure 2b). Milling of the BG powder (Figure 2c) led to similar smaller plate like morphology with a medium particle size of d_{50} = 1.61 µm, as determined by laser diffraction measurements. The milled BG powder showed more agglomerations when compared to the milled and PTES coated BG sample (compare Figure 2 c and d). EDX investigations showed elemental Aluminium (Al) content in the milled powders. This can be attributed to contamination from the milling process inside an alumina milling beaker with alumina balls. EDX characterization of all samples showed a reduced Na content in the surface of the treated BG samples compared to the as-purchased sample (data not shown) and no significant changes in Si, Ca and P content.

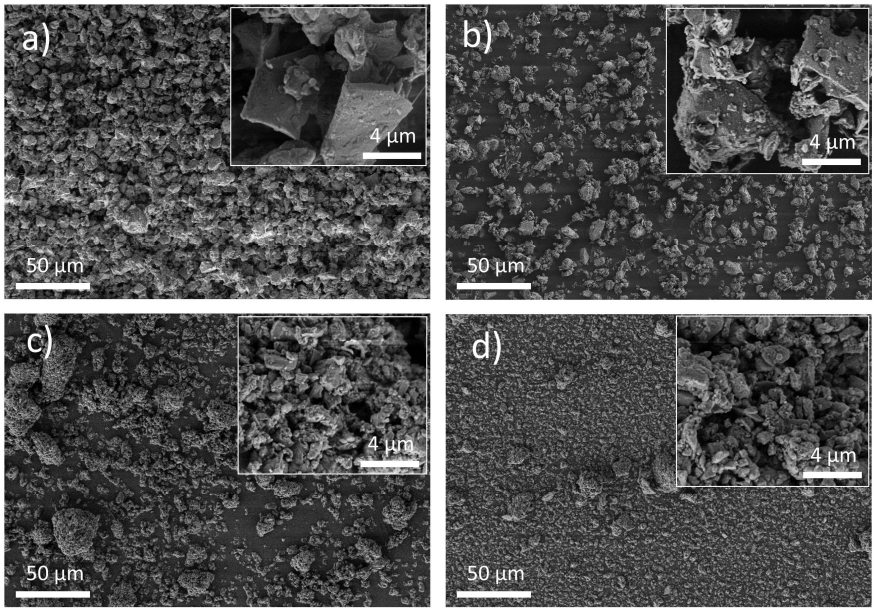

Figure 2: Scanning electron micrographs of BG powders after different treatments a) as-purchased BG b) PTES coated BG c) milled BG and d) milled and PTES coated BG. Large scale micrographs represent overviews (scale bar = 50 µm), inset micrographs are higher resolution (scale bar = 5 µm).

X-ray fluorescence analysis (XRF) revealed a changed composition of the BG after milling in water with a reduced Na_2O content of 20.7 wt.%. The other constituent ratios were as follows: 47.0 wt.% SiO_2, 26.6 CaO and 5.7 P_2O_5. Since milling of the BG was performed for 30 minutes in water surface near Na^+ ions will likely be released from the glass network into the milling medium, which will lower the Na_2O content in the glass [13].

FT-IR investigations (Figure 3) of the milled and PTES coated BG in comparison with pure PTES and as purchased BG 45S5 showed that the complete treatment of the BG did not influence the BG structure. Typical bands of bioactive glass, such as Si-O stretching at ~1000 cm^{-1} and ~910 cm^{-1} for non-bridging oxygens [14], as well as bands at 500 – 420 cm^{-1} characteristic for rocking vibrations and at ~750 cm^{-1} for bending vibrations both in bridging oxygens of the network [15] were present in the as-purchased BG and the milled and PTES-coated BG. In addition to the typical BG small bands between 2960 and 2870 cm^{-1} were visible after PTES treatment, which can be attributed to various CH groups [16]. As they are not visible in the as-purchased sample (Figure 3 right for magnified spectra) this indicates the formation of Si-O-CH_3 and Si-O-R groups in the surface of the BG after PTES treatment. The intensities are low, as we only used 1.0 wt.% of PTES in the wet-coating process.

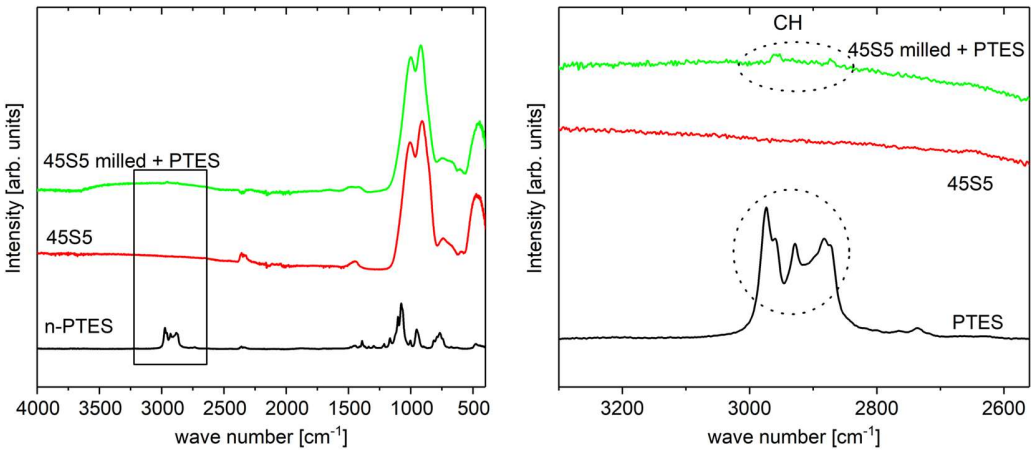

Figure 3: ATR-FTIR spectra of PTES, as purchased 45S5 and milled and PTES coated 45S5 (left) and magnified spectra of these samples ranging from 3300 to 2600 cm^{-1}.

3.2 Production of composite microspheres

3.2.1 Incorporation study

Figure 4 illustrates the influence of BG modifications, such as milling and PTES coating, on the morphologies and specific surface area (SSA) of composite particles produced by the solid-in-oil-in-water emulsion method. As can be seen in Figure 4a the sample produced with as-purchased BG as a porogen shows spherical PLGA particles with a high porosity and small particles adhering to some parts of the spheres. When using BG coated with the coupling agent PTES, the large microparticles were less porous on the outside with more small particles adhered to the surface (Figure 4b). With milled BG (Figure 4c) we achieved porous PLGA spheres with smaller pores compared to the samples shown in Figure 4a. The sample with milled and PTES coated BG shows spheres without obvious porosity and a rough surface with fine particles adhering to the polymer. The SSA increased more than 3x with milling of the BG, while coating of the BG samples led to a reduction in SSA of ~23 % compared to the uncoated samples.

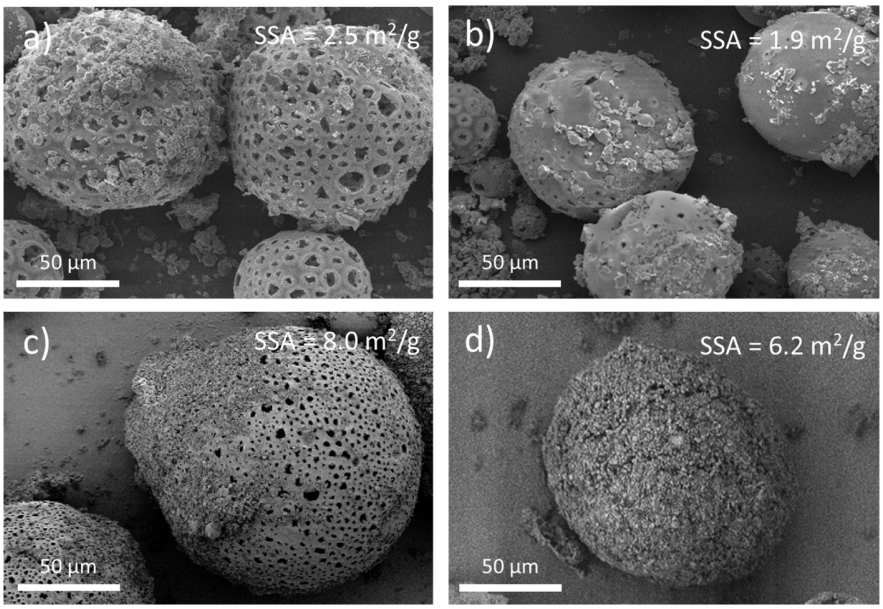

Figure 4: SEM images of incorporation test of BG particles into the polymer matrix with a) as-purchased BG d_{50}=3,90 µm, b) PTES coated BG d_{50}=3,90 µm, c) milled BG d_{50}=1,61 µm, and d) milled and PTES coated BG d_{50}=1,61 µm. The images a) to d) show the change in morphology of the spheres produced via s/o/w emulsion method using BG with different properties (size and coating) and their specific surface area (SSA) measured using BET.

Elemental mapping of a composite sample with milled and PTES coated BG revealed Si and Na uniformly distributed across the particle surface, indicating that the surface contains uniformly distributed BG particles (Figure 5).

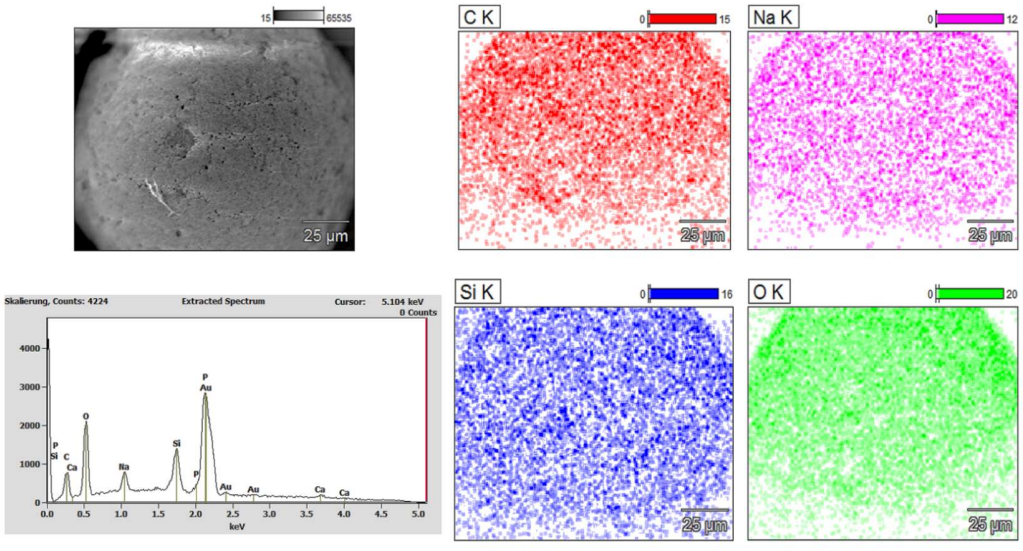

Figure 5: EDX mapping of a microsphere surface with PLGA:BG composition of 50:50. This shows a composite particle with milled and PTES coated BG as porogen. While the PLGA consists exclusively of the elements carbon, hydrogen and oxygen, BG contains silicon and sodium among others. Thereby it can be assumed that the investigated particle contained BG powder on the surface.

Particle size distribution measurements (Figure 6) confirm the results of SEM images for the incorporation test - the overall particle size distribution for all four samples is relatively similar. The most significant differences in the distributions can be found below 16 µm grain size. Composite powders with as-purchased and PTES coated BG showed a distinct bimodal particle size distribution with maxima at 80 – 90 µm for composite particles and ~8 µm. This can be attributed to BG particles that have not been incorporated especially as all curves show small maxima in the size range attributed to the size of the respective BG particles used. The least number of particles below 10 µm can be found in the sample with milled and coated BG.

The combination of milling and subsequent coating with PTES showed the most promising composite particles (as these had a relatively closed outer surface), therefore this BG treatment was chosen to produce composite powders for LS processing.

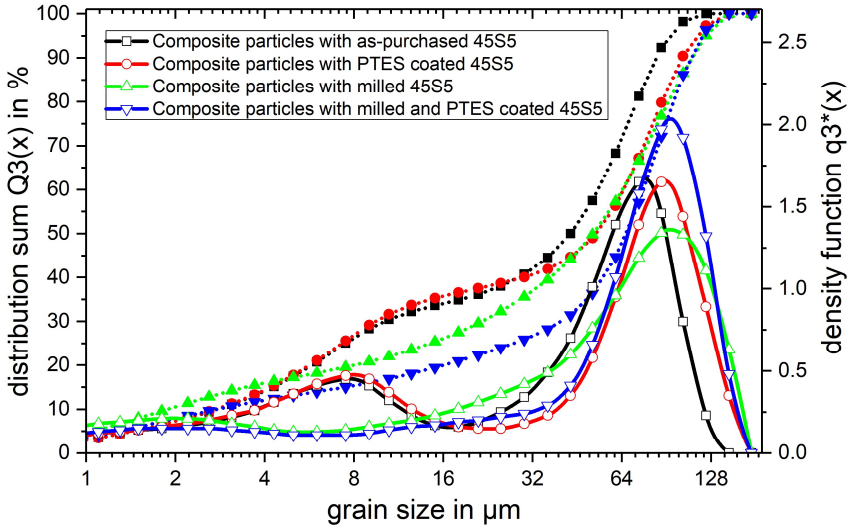

Figure 6: Particle size distribution of composite powders produced by s/o/w emulsion method. The used BG was treated differently for each sample. Black: BG as purchased, red: PTES coated BG, green: milled BG, blue: milled and PTES coated BG. Filled symbols with dotted lines correspond to the distribution sum (left y-axis), and blank symbols with continued lines correspond to the density function (right axis).

3.2.2 Powders for LS-Process with varying PLGA:BG ratios

Figure 7 illustrates the influence of the amount of the BG solid phase (d_{50} = 1.61 with PTES coating) on composite particles in the s/o/w emulsion method. Varying the PLGA:BG weight ratio (100:0, 80:20, 67:33 50:50) resulted in a change of particle morphology. As can be seen in Figure 7a and b the O/W emulsion set-up produced pure PLGA microspheres with smooth surfaces and high degree of sphericity. While the sample with 20 % BG (b) shows a high degree of sphericity, adding more BG resulted in less spherical particles (c and d). Moreover, the morphologies of the samples with 33 % and 50 % BG also resulted in larger particles that have been broken up in the production process. The non-spherical particles especially from the 67:33 and 50:50 samples showed a dough like morphology with rough surfaces.

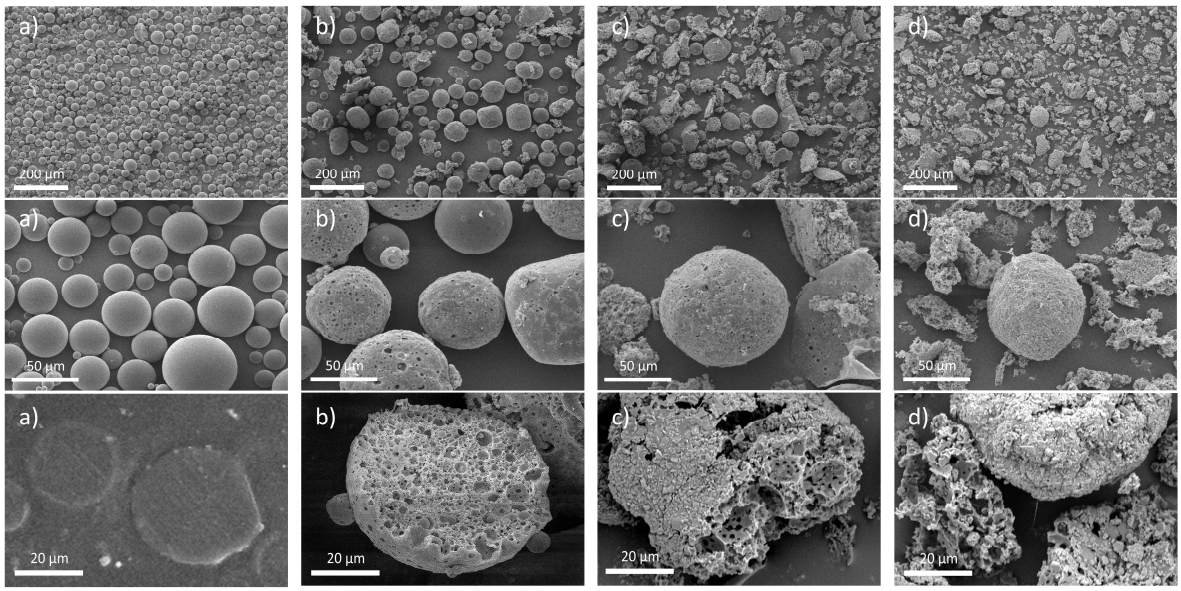

Figure 7: SEM images of particles with different PLGA:BG ratios with a) 100:0, b) 80:20, c) 67:33 and d) 50:50. The medium row shows higher magnification of the particles. The images in the bottom row show cross sections of single powder particles (with the particles of the 100:0 sample embedded in epoxy resin). Depending on BG content the samples showed different morphologies and porosities.

Particle size investigations of the composite powders (Figure 8) showed a relation between BG content and particle size distribution of the produced powders. All particle size distributions are unimodal. Pure PLGA powder has a narrow particle size distribution with a maximum at 50 µm and 90 % of all particles are smaller than 60 µm. The sample containing 20 % BG shows a wider particle size distribution ranging from 4 to 128 µm with a maximum at 55 µm. 90 % of all particles are smaller than 70 µm. For the 67:33 powder the maximum is shifted to 65 µm, the particle size distribution is similar to the 80:20 powder, 90 % of all particles are smaller than 85 µm. For the powder with 50 % BG content the maximum shifted to 95 µm, the particle size distribution ranges between 8 and 135 µm. This confirms the qualitative SEM results by showing that in relation to the BG content the particle size varies widely.

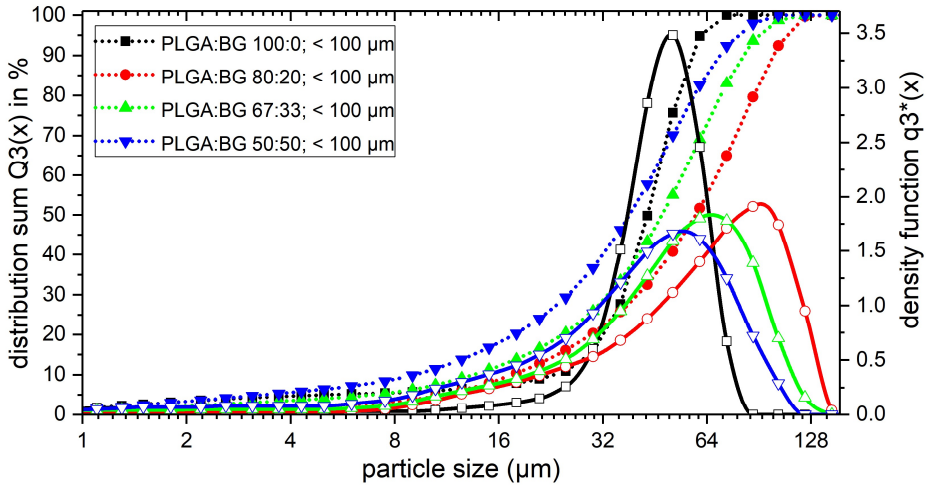

Figure 8: Particle size distribution of powders produced for LS experiments. Filled symbols with dotted lines correspond to the distribution sum (left y-axis), and blank symbols with continued lines correspond to the density function (right axis).

3.2.3 PLGA:BG content in LS-powders

TG analysis of the powders showed good accordance between weight loss at 600 °C, which can be attributed to the organic polymer content in the composite particles (Table 1). For pure PLGA RG755S Evonik gives an ash content of smaller or equal to 0,10 %. Contrary to that we found a mass loss of 96,2 % at 600 °C, which we used to calculate the PLGA:BG ratios of the other samples by multiplying this value with the mass loss of the composite powders (assuming only the polymer decomposes until 600 °C). These results indicate that the PLGA:BG ratio is not changed to a large degree during powder production and especially washing.

Table 1: Thermogravimetric analysis studying incorporation behaviour and specific surface area of powders (calculated from particle size and measured).

Sample composition PLGA:BG	Weight loss at 600 °C in %	Calculated PLGA:BG ratio from TG data in %	d_{32} in µm from particle size measurements	Sm in m^2/g calculated using d_{32} and (composite) densities	Specific surface area (SSA) from BET in m^2/g
100:0	96.1	100 : 0	13.7	0.336	0.1
80:20	83.6	80.3 : 19.7	59.3	0.069	9.6
67:33	65.8	63.3 : 36.7	54.4	0.070	7.4
50:50	50.9	48.9 : 51.1	41.8	0.082	6.2
0:100*	-	-	1.8	1.208	5.9

*This includes the values of the milled and PTES coated BG, which were not characterised by TGA.

3.3 Surface measurement and comparison with surface calculation

3.3.1 Calculation of powder surface

Besides measuring the SSA by nitrogen adsorption, the theoretical surface area of the powders was calculated. For this it was assumed that all powders have only spherical particles using the formula for the surface per unit mass of a powder $S_m = \frac{6}{\rho d}$ [17] where ρ is the density of the material and d the diameter of the spheres and substituting the diameter d with a statistical diameter for powder particles (to model the multidisperse powders) – the mean volume-surface diameter or sauter mean diameter $d_{32} = \frac{\sum_{k=1}^{n} nd^3}{\sum_{k=1}^{n} nd^2}$ [18] (which can be described for a specific particle-size distribution (PSD) as follows: if one was to transform the whole volume of all relevant particles in a PSD into spheres of equal size, the diameter of the spheres with equal size would be the sauter mean diameter) where n is the number of particles in a mass powder and d the diameter of the n particles, ending with the equation for S_m:

$$S_m = \frac{6}{\rho} * (\frac{\sum_{k=1}^{n} nd^2}{\sum_{k=1}^{n} nd^3})$$

3.3.2 Comparison of S_m and SSA

Comparing S_m and SSA for the non-composite materials a significant difference for both the pure PLGA and pure BG system can be noted. Generally, the pure PLGA system's morphology fits well the assumptions for the calculation, so the deviation from the SSA measurement by more than twofold might either be explained by an underestimation of d_{32} from the particle size analysis or a high error of the SSA due to using a powder with very small surface. For the pure BG the deviation could be a result of the fragmented shape of the particles that was non-spherical as a result of the milling process and an overestimation of d_{32} as a result. For the composite powders the assumption of the S_M calculation does not fit the powders real morphology as the powders porosity is not taken into account. However, the values for S_M give a good indication that even though d_{32} is decreased with more BG, S_M rises because of the increased density.

3.4 Packing properties and powder flowability / compressibility

3.4.1 Packing densities

Dealing with composite powders with changing composite densities it is not obvious to compare bulk and tapped densities directly as these are dependent on the powders material density. For this reason in Figure 9 normalised values, the packing density for bulk packing $f_{bulk} = \frac{\rho_{bulk}}{\rho_M}$ as well as for tapped packing $f_{tapped} = \frac{\rho_{tapped}}{\rho_M}$ were calculated. The composite density ρ_M was calculated with $\frac{1}{\rho_M} = \frac{W_1}{\rho_1} + \frac{W_2}{\rho_2}$ [19] (ρ_1 and W_1 is the density and weight ratio of part 1 and ρ_2 and W_2 of part 2) using the theoretical densities of PLGA 1,3 g/cm^3 and 2,7 g/cm^3 for BG. In Figure 9 the bulk and tapped densities (green) and the bulk and tapped packing (yellow) of the 100:0 powder was aligned which makes obvious that there is no clear trend for the packing to change if the composition is changed. The composite powders with BG contents ranging from 20 to 50 wt.% show low packing densities which can be attributed to the varying porosity and morphology of these powders (Figure 7 b to d). The 100:0 pure PLGA powder particles with their high degree of roundness, high theoretical density and smooth surfaces (Figure 7 a) show a bulk packing

of 47.46 %. This is a high value for any free-flowing polymeric powder considering the standard polymeric LS powder (EOSINT 2200) which has a bulk packing density of 40.74 % (calculated using ρ_{bulk} = 0.44 g/cm^3, data given by EOS GmbH).

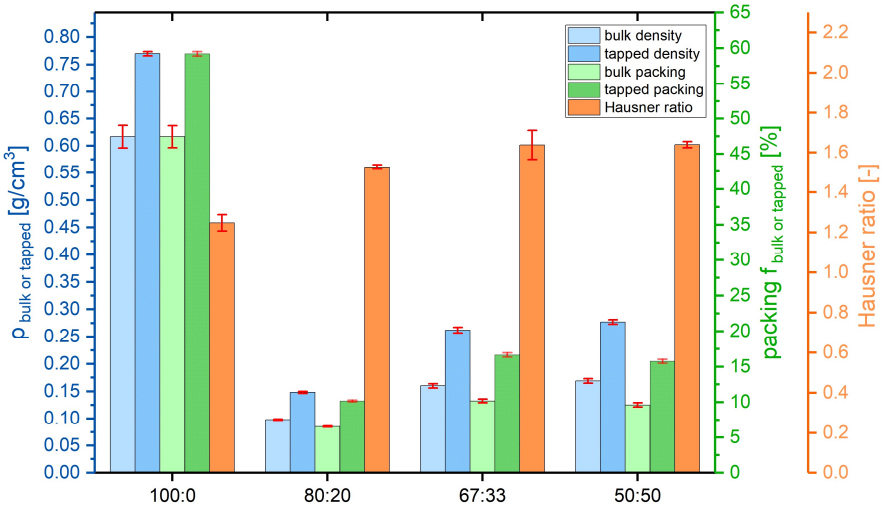

Figure 9: Bulk density, tapped density, bulk packing, tapped packing and Hausner ratio of produced powders.

3.4.2 Powder compressibility assessment

The Hausner ratio (HR) is a value of the compressibility of a powder which is used to evaluate powder flowability (HR < 1.11: excellent flow; 1.12–1.18: good flow; 1.19–1.25: fair flow; 1.26–1.34: passable flow; 1.35–1.45: poor flow; 1.46–1.59: very poor flow; >1.60: no flow [20]) assuming that poorly flowing powders pack with relatively large voids and are therefore more compressible [21]. We observed (Figure 9) that while the HR for pure PLGA powder falls in the category of "fair flow" which fits to our experience while handling the powder, the Hausner values for the composite powder would indicate "very poor flow" / "no flow" for all composite powders -this was contrary to our experience while handling the powder and is a hint, that the composite powders are deformed during the tapped density measurements (see discussion).

3.5 LS samples from composite microparticles

An example of the microstructure produced by LS can be seen in the SEM images from the 80:20 sample in Figure 10. All samples from LS processing of porous powders resulted in specimens that showed a highly porous structure (also see X-ray tomographic data in Figure 11). Because of their high porosity, the samples had low mechanical strength, which was a problem when handling the samples. For the 80:20 sample the structure consists of more or less rounded nodes that are connected by a web of material bridges. In Figure 10a the line-shaped pattern of the material bridges can be seen, which is due to the line wise movement of the laser beam. With higher BG content the visible porosity is reduced (Figure 10b and c) and the sample surfaces look more finely structured. The line shaped surface morphology indicating the sintering lines is no longer visible for 67:33 and 50:50 composite powders. In higher resolution single spherical particles are visible, as well as small particles resembling the morphology of the bioglass particles. The surface structure of the 80:20 sample is smoother than that of the other samples, which can be attributed to the higher PLGA content which was melted during the LS process. EDX of all samples (data not shown) confirmed BG content in all three compositions.

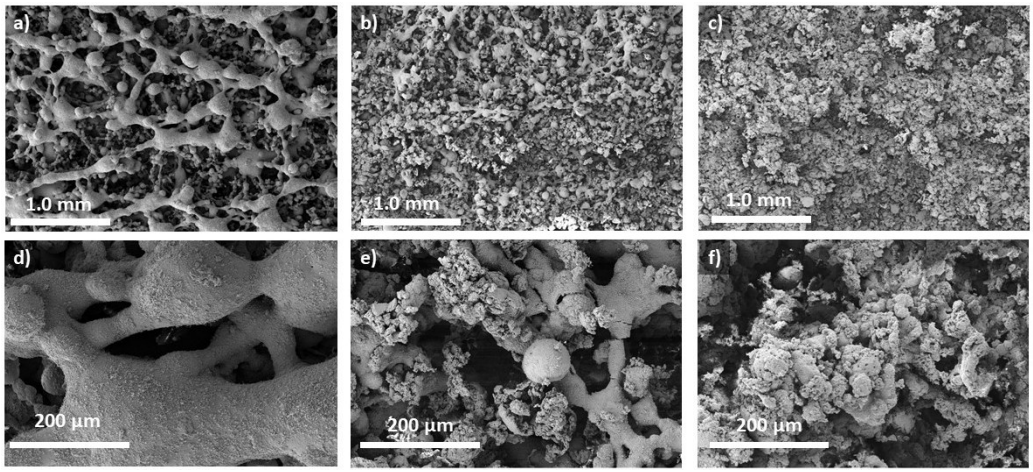

Figure 10: SEM images of the LS samples from composite microparticles with a PLGA:BG ratio various compositions. Image a) low resolution image of the 80:20 sample, b) 67:33 sample and c) 50:50 sample. Corresponding higher resolution images in second row of d) 80:20 sample, e) 67:33 sample and f) 50:50 sample.

Using X-ray tomographic analysis on the LS Parts we found a total porosity (open plus closed porosity) of all three LS Parts to be quite similar with 74,7 % for the 80:20 powders, 73,7 % for 67:33 and 76,1 % for 50:50.

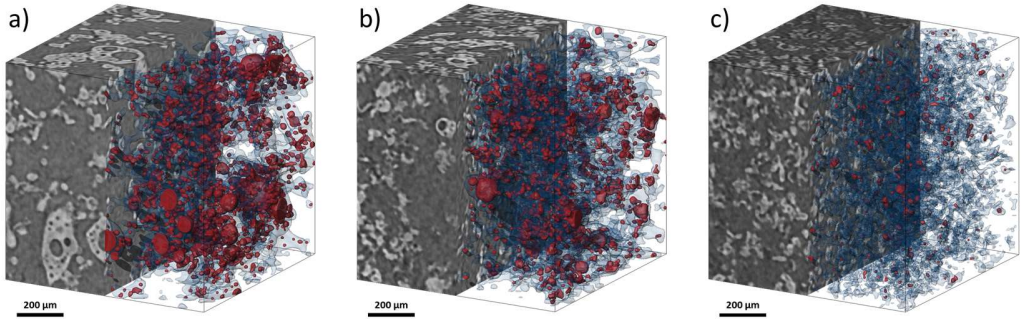

Figure 11: X-ray tomographic data of composite LS samples produced from powders with varying PLGA:BG ratios with a) 80:20, b) 67:33 and c) 50:50. The left side of each cube shows the cross section of the sample and the right side a visualisation of the open and closed porosity, blue being the composite material, red the closed porosity and clear / white the open porosity.

However, Figure 11 makes obvious that there are significant differences regarding the closed porosity: The highest closed porosity was found with 3.7 % for the 80:20 sample, the 67:33 powder had 1.7 % and almost no closed porosity was found for the 50:50 sample which had a closed porosity of 0.2 %. From Figure 12 we conclude that the 80:20 powder produced not only the highest closed porosity but also the biggest closed pores of all samples, which corresponds well to the impression derived from the SEM characterization of the LS samples (Figure 10).

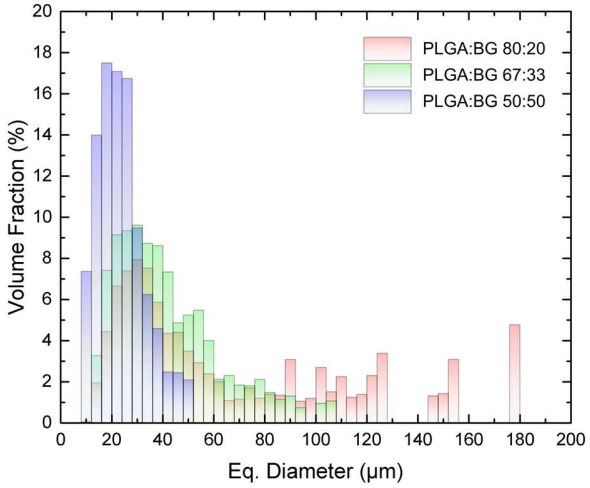

Figure 12: Pore size distributions of closed pores from X-ray tomographic data for the LS parts.

4. Discussion

Successful incorporation of BG into the PLGA matrix was achieved after milling and surface coating of the BG with PTES (a biocompatible silane). Of the two, the silane coating seems to be the more efficient parameter. Due to the high surface energy of inorganic materials such as BG and HA and low surface energy of polymer materials it is difficult to form a good interface between PLGA matrix and inorganic filler material [22]. Additionally for the production of composite microspheres through an emulsion process hydrophilic inorganic particles are highly likely to move from the oil or solvent phase into the water phase during the emulsion process [23], thereby leaving behind porous PLGA particles separated from the glass particles, as can be seen in Figure 4 for our incorporation experiments with as-purchased and only milled BG. Coating BG with PTES therefore led to grafting a hydrophobic surface layer onto the BG particles, which help introduce a covalent bond between BG and PLGA matrix. With this method we were able to incorporate up to 50 wt.% of inorganic BG into composite particles. Increased BG content influenced the composite particle morphology strongly. Pure PLGA particles showed spherical morphology with a relatively narrow particle size distribution with a maximum around 50 µm and d_{90} below 60 µm. With increasing BG content up to 50 wt.% the initial spherical morphology was lost, and the particles became larger in average [24]. In addition, SEM and nitrogen adsorption measurements indicated that lower BG contents led to more porosity inside the particle, as composite particles with 20 wt.% BG had a specific surface area of 9.6 m^2/g, 50:50 composite particles had a SSA of 6.2 m^2/g. Generally, all composite powders showed open porosity and a high SSA - it is noteworthy that the decreasing SSA with increasing BG content indicates that there is a complex foaming process happening as less BG (80:20) produced powders with the highest open porosity.

4.1 Packing

This increased porosity inside the composite particles with lower BG content also led to lower bulk density and packing, as compared to composites with higher loading (67:33 and 50:50 samples). With higher BG contents the bulk density was increased from 0.10 g/cm^3 in the 80:20 sample to 0.15 and 0.16

g/cm³ for 33:67 and 50:50 composite samples respectively. All composite powders showed an increase from bulk to tapped density of around 50 %, indicating good powder compressibility. The Hausner ratio which is derived from the relation between bulk and tapped density, indicated “fair” flowability of the pure PLGA powder, and “very poor” to “no flow” flowability for all composite powders. This is contrary to our observation that all composite powders flow reasonably well. The discrepancy could indicate that the individual composite particles are not very stiff and can be compressed due to their porosity, therefore in this case the Hausner ratio should be viewed as a measure for the powder compressibility and not so much for the flowability.

4.2 Laser sintering

Laser sintering of the composite powders confirmed the low powder packing, as it produced highly porous structures independent of the BG content. Overall porosity was around 75 % for all three composite powders. The closed porosity content decreased with increasing BG content, the 20:80 sample showed the largest closed pores, when investigated by µCT. A similar microstructure (with no mention of pronounced sintering lines) has been reported for LS parts made from cryogenically milled PCL powder beds [25]. As well as in our approach we assume both microstructures to be a result of the low powder bed packing densities, in our case not from the low packing of the single particles (which should have been relatively high, as a result of their spherical shape) but from the foamed microstructure of the particles themselves. We assume for our microstructure that laser-powder interaction leads to liquid phase sintering e.g. a kind of a melt pool as the thin polymer walls of the foamed PLGA were heated by the laser and a dense polymer matrix with embedded particles was produced. Such a sintering behaviour could also explain the high closed porosity (3.7 %) of the 80:20 powder compared to the other powders, as this powder showed the highest SSA (Table 1), has relative to the other composite powders the lowest packing density e.g. the highest porosity (Figure 9) and can therefore be assumed to have the thinnest PLGA wall structures, which would melt relatively fast entrapping gas into closed pores.

5. Conclusions

In the first part of this work we report on the modification of the porogen BG using milling and coating which enabled us to produce porous microparticles with BG incorporated into or onto the foamed PLGA spheres. In the second part we investigate the production of such porous composite particles for LS with different macro/microstructures, varying specific surface areas and powder packing properties. In the future such powders could be useful for various applications in medicine where large surface areas and or low density particles made of resorbable polyesters and incorporated BG porogen are needed for example as carriers for drugs, absorption and desorption of substances, pulmonary drug delivery and tissue regeneration [26]. In the third part we report on the use of these porous particle powders as feedstock for laser sintering experiments that produced extra porous structures with overall porosities between 73,7 % and 76,1 % and varying degrees of closed porosity from 0,3 % to 3,7 %. The best results were achieved with 80:20 powders that showed particles with high sphericity, the largest SSA (of the LS powders), and a wide laser processing window. Furthermore, (even though we did not conduct standardised mechanical tests for the LS parts) we found the 80:20 parts to be the most mechanically stable (judging from handling). While the low mechanical properties of the LS parts inhibit a use in load bearing applications our approach could be useful on the one hand in LS processing with multiple feedstock powders where the porous powder would be used to fill geometries that have a hard outer shell (similar to foaming inside an already produced geometry) or on the other hand to produce porous tissue engineering scaffolds with closed pores.

6. Acknowledgements

The authors acknowledge Petra Marsiske for XRF, Christina Eichenauer for BET and Heinz Sap for FTIR, all from TU Berlin. David Karl would like to thank the Evonik Stiftung for their financial support. This work was supported by TU Berlin through an internal funding agent (Jahreskonzepte 2017; Project number: 60330018).

7. Data availability

The raw data required to reproduce these findings will be made available on request.

8. References

[1] A.L. Dumitrescu, Chemicals in surgical periodontal therapy, Springer, Heidelberg, 2011.

[2] M. Epple, Biomaterialien und Biomineralisation: Eine Einführung für Naturwissenschaftler, Mediziner und Ingenieure, 1st ed., Teubner, Stuttgart, Leipzig, Wiesbaden, 2003.

[3] A. Hoppe, N.S. Güldal, A.R. Boccaccini, A review of the biological response to ionic dissolution products from bioactive glasses and glass-ceramics, Biomaterials 32 (11) (2011) 2757–2774. https://doi.org/10.1016/j.biomaterials.2011.01.004.

[4] D.L. Wheeler, M.J. Montfort, S.W. McLoughlin, Differential healing response of bone adjacent to porous implants coated with hydroxyapatite and 45S5 bioactive glass, Journal of biomedical materials research 55 (4) (2001) 603–612. https://doi.org/10.1002/1097-4636(20010615)55:4<603:AID-JBM1054>3.0.CO;2-N.

[5] A. Stamboulis, L.L. Hench, A.R. Boccaccini, Mechanical properties of biodegradable polymer sutures coated with bioactive glass, Journal of materials science. Materials in medicine 13 (9) (2002) 843–848. https://doi.org/10.1023/A:1016544211478.

[6] M. Vallet-Regí, Bioceramics with clinical applications, John Wiley & Sons Inc, Chichester, West Sussex, Hoboken, NJ, 2014.

[7] R.M. German, Particle packing characteristics, Metal Powder Industries Federation, Princeton NJ, 1989.

[8] G. Jiang, M.E. Evans, I.A. Jones, C.D. Rudd, C.A. Scotchford, G.S. Walker, Preparation of poly(epsilon-caprolactone)/continuous bioglass fibre composite using monomer transfer moulding for bone implant, Biomaterials 26 (15) (2005) 2281–2288. https://doi.org/10.1016/j.biomaterials.2004.07.042.

[9] R.O. Grey, J.K. Beddow, On the Hausner Ratio and its relationship to some properties of metal powders, Powder Technology 2 (6) (1969) 323–326. https://doi.org/10.1016/0032-5910(69)80024-0.

[10] DIN EN ISO, Plastics - Determination of apparent density of material that can be poured from a specified funnel (DIN EN ISO 60:1999), Beuth Verlag, Berlin, 2000.

[11] F. García-Moreno, C. Jiménez, P.H. Kamm, M. Klaus, G. Wagener, J. Banhart, C. Genzel, White-beam X-ray radioscopy and tomography with simultaneous diffraction at the EDDI beamline, Journal of synchrotron radiation 20 (Pt 5) (2013) 809–810. https://doi.org/10.1107/S0909049513018670.

[12] W. van Aarle, W.J. Palenstijn, J. Cant, E. Janssens, F. Bleichrodt, A. Dabravolski, J. de Beenhouwer, K. Joost Batenburg, J. Sijbers, Fast and flexible X-ray tomography using the ASTRA toolbox, Optics express 24 (22) (2016) 25129–25147. https://doi.org/10.1364/OE.24.025129.

[13] E. Verne, C. Vitale-Brovarone, E. Bui, C.L. Bianchi, A.R. Boccaccini, Surface functionalization of bioactive glasses, Journal of biomedical materials research. Part A 90 (4) (2009) 981–992. https://doi.org/10.1002/jbm.a.32153.

[14] J. Serra, P. González, S. Liste, C. Serra, S. Chiussi, B. León, M. Pérez-Amor, H.O. Ylänen, M. Hupa, FTIR and XPS studies of bioactive silica based glasses, Journal of Non-Crystalline Solids 332 (1-3) (2003) 20–27. https://doi.org/10.1016/j.jnoncrysol.2003.09.013.

[15] M. Araújo, R. Viveiros, A. Philippart, M. Miola, S. Doumett, G. Baldi, J. Perez, A.R. Boccaccini, A. Aguiar-Ricardo, E. Verné, Bioactivity, mechanical properties and drug delivery ability of bioactive glass-ceramic scaffolds coated with a natural-derived polymer, Materials science & engineering. C, Materials for biological applications 77 (2017) 342–351. https://doi.org/10.1016/j.msec.2017.03.169.

[16] G.F. Andrade, D.C.F. Soares, R.G. dos Santos, E.M.B. Sousa, Mesoporous silica SBA-16 nanoparticles: Synthesis, physicochemical characterization, release profile, and in vitro cytocompatibility studies, Microporous and Mesoporous Materials 168 (2013) 102–110. https://doi.org/10.1016/j.micromeso.2012.09.034.
[17] I.G. Shatalova, N.S. Gorbunov, V.I. Likhtman, Physiocochemical principles of vibratory compacting, in: K. Roll, P.K. Johnson (Eds.), Vibratory Compacting: Principles and Methods, Plenum Press, 1967, pp. 1–206.
[18] DIN ISO, Representation of results of particle size analysis – Part 2: Calculation of average particle sizes/diameters and moments from particle size distributions (ISO 9276-2:2014), Beuth Verlag, Berlin, 2018.
[19] R.M. German, S.J. Park, Mathematical relations in particulate materials processing: Ceramics, powder metals, cermets, carbides, hard materials, and minerals, Wiley, Hoboken, NJ, 2008.
[20] A. Zocca, C.M. Gomes, A. Staude, E. Bernardo, J. Günster, P. Colombo, SiOC ceramics with ordered porosity by 3D-printing of a preceramic polymer, J. Mater. Res. 28 (17) (2013) 2243–2252. https://doi.org/10.1557/jmr.2013.129.
[21] D. Schulze, Powders and bulk solids: Behavior, characterization, storage and flow, Springer, Berlin, New York, 2008.
[22] F. Xin, C. Jian, R. Jianming, Z. Zhongcheng, Z. Jianpeng, Effects of Surface Modification on the Properties of Poly(lactide-co-glycolide) Composite Materials, Polymer-Plastics Technology and Engineering 48 (6) (2009) 658–664. https://doi.org/10.1080/03602550902824523.
[23] X. Qiu, Y. Han, X. Zhuang, X. Chen, Y. Li, X. Jing, Preparation of nano-hydroxyapatite/poly(l-lactide) biocomposite microspheres, J Nanopart Res 9 (5) (2007) 901–908. https://doi.org/10.1007/s11051-006-9158-6.
[24] X. Shi, Y. Wang, L. Ren, Y. Gong, D.-A. Wang, Enhancing alendronate release from a novel PLGA/hydroxyapatite microspheric system for bone repairing applications, Pharmaceutical research 26 (2) (2009) 422–430. https://doi.org/10.1007/s11095-008-9759-0.
[25] G.V. Salmoria, D. Hotza, P. Klauss, L.A. Kanis, Roesler, C. R. M., Manufacturing of Porous Polycaprolactone Prepared with Different Particle Sizes and Infrared Laser Sintering Conditions: Microstructure and Mechanical Properties, Advances in Mechanical Engineering 6 (0) (2014) 640496. https://doi.org/10.1155/2014/640496.
[26] Y. Cai, Y. Chen, X. Hong, Z. Liu, W. Yuan, Porous microsphere and its applications, International journal of nanomedicine 8 (2013) 1111–1120. https://doi.org/10.2147/IJN.S41271.